

Modified split-potential model for modeling the effect of DBD plasma actuators in high altitude flow control



M. Abdollahzadeh^{*}, J.C. Páscoa, P.J. Oliveira

Universidade da Beira Interior, Departamento de Engenharia Electromecânica, C-MAST – Center for Mechanical and Aerospace Sciences and Technologies, FCT (Portuguese Foundation for Science and Technology) Research Unit No. 151, Covilhã, Portugal

ARTICLE INFO

Article history:

Received 17 February 2014

Received in revised form

4 May 2014

Accepted 28 May 2014

Available online 10 June 2014

Keywords:

DBD system capacitance

Semi-empirical

Thrust estimation

Body force

Barrier discharge

Flow control

ABSTRACT

Surface DBD plasma actuators are novel means of actively controlling flow. They have shown promising ability in reducing drag, postponing transition from laminar to turbulent flow, suppression of separation, noise reduction and enhancement of mixing in different applications. The CFD simulation of the effect of plasma actuator in such kind of applications could provide more information, and insight, for optimization and design of close looped flow control systems. However, the fluid models for simulating the formation of the plasma and its effect are computationally expensive such that, although they provide more detailed information about the physics related to the formation plasma, they are still not viable to be used in large scale CFD simulations. In this paper, we present the modified version of a simpler model that predicts the thrust generated by the plasma actuator with acceptable accuracy and can be easily incorporated in CFD calculations. This model is also free of empirical fitting parameters, being based on pure flow physics scaling.

© 2014 Elsevier B.V. All rights reserved.

1. Introduction

Dielectric Barrier Discharge (DBD) plasma actuators gained increased interest during the past decade for different applications [1–4]. It has been proven that they have a promising potential for controlling flow in diverse applications. Many experimental and numerical works have been done for the purpose of better understanding the mechanisms by which these kind of actuators influence the flow and also for the optimization of their design and improvement of their performance [5–7]. DBD plasma actuators mostly influence the flow through two different mechanisms, depending on the type of the excitation voltage shape employed. If the DBD plasma actuator is excited through a nano-second voltage pulse, the characteristics of the flow around the DBD actuator is altered through fast energy deposition and creation of micro shock-waves. In contrast, if some kind of radio frequency excited voltage is used, the flow will be accelerated around the actuator plate due to the formation of ionic wind.

The plasma fluid model [8–11] and the particle in cell model [12] are the most sophisticated and common models for simulating plasma actuators. However, due to large difference between the

spatial and temporal scales of the flow and the plasma, the computational time of these techniques is excessively high. Even with multi-processor modeling approaches and some kind of unsteady acceleration techniques [13], such as adaptive local time stepping. The solution of large scale problems in realistic geometries is not viable with those models. A more simplified approach needs to be devised in order to have both acceptable accuracy and fast simulation times.

In this aspect, a semi-numerical modeling of the effect of plasma actuator could provide a rapid tool to ascertain the effect of plasma actuators. Different such numerical models have been proposed, including semi-experimental [14,15], basic phenomenological models [16–23] and PIV measurement-based models [24–27]. Obviously, the accuracy of the simulation results reduces when the simplicity of models is increased. However, high fidelity fluid models are too much computationally expensive to be used for simulation of large scale problems. PIV data based models also need availability of complex experimental results for the tested plasma actuator. Moreover, since the major influence of the DBD actuator occurs at large scales, such as energy deposition and ionic field, the overall effect could be captured by simpler phenomenological models.

Different simplified models can be found in the literature. Shyy et al. [28] considered a body force formulation. The electric field region was confined to a triangular shaped region over the actuator

^{*} Corresponding author. Tel.: +351 925467631 (mobile).

E-mail address: mm.abdollahzadeh@yahoo.com (M. Abdollahzadeh).

plate, whose size was estimated by the length of the actuator and an assumed value for the height of the plasma region. The maximum body force in that model would occur at the edge of the exposed electrode and this body force was directed parallel to the shape of the body force region. The height of the plasma region and a constant charge density were considered to be the fitting parameters of the model. Suzen et al. [29] developed a model assuming a Gauss law, by additionally considering the electric potential to be produced by the accumulated charge density over the dielectric surface to obtain the charge density distribution. The distribution of the charge density was assumed to be Gaussian in accordance to the observed experimental distribution. Scales for the space charge density (maximum charge density), shape factors of the Gaussian distribution, and Debye length were selected to match experimental results. Both these models were not able to accurately capture the applied voltage-thrust dependency which was observed experimentally by [30] to be $U_{\max} \propto V_{\text{app}}^{7/2}$.

An involved unsteady phenomenological model was presented by Orlov et al. [20], who considered the DBD actuator system as an electric circuit with several electric components, including capacitances and resistances. In this way, they were able to calculate the so called memory voltage over the surface of the dielectric layer. The model successfully predicted the ratio of the voltage-thrust dependency. However, the value of the body force was too much over estimated in comparison to experimental results. Mertz [21] modified the model presented by Orlov et al. to increase the accuracy of the direction of the predicted induced flow. These models required some parameters, such as plasma resistivity and plasma height which were fitted to match experimental results. Recently, Lemire et al. [31] developed a hybrid model, by estimating the charge density distribution over the embedded electrode as in the model of Suzen et al., and by considering the virtual electrode concept from the circuit model of Orlov et al.

Although the above mentioned models have gained success in modeling some experimental cases, as shown by Palmeiro [32], their predictive capability varies significantly depending on particular experimental situations. Moreover, most of them involve fitting parameters that need to be predefined by observing experimental results. These aspects restrict their practicality as a tool for the purpose of designing and testing flow control applications for which experimental results are not available. In the present paper, we wish to propose a modification to the model presented in Ref. [29]. This modification will serve to reduce the dependency of the results on fitting parameters, to capture correctly the voltage-thrust dependency, and to increase the range of validity of the model for different experimental situations.

2. Modified split-potential model

In this section we will present the modification to the split-potential model. The model is modified through scaling the

components of the body force (Section 2.1) and introducing these new scales in the split-potential model to simulate body force distribution generated by the plasma.

2.1. Scaling of generated thrust and body force

The thrust produced by the DBD plasma actuator is proportional to the power consumption of the DBD actuator system. For estimating the scale of power consumption the dielectric barrier discharge actuator is regarded as an AC circuit having a capacitor. Two cylindrical capacitors are considered, similarly to the work of Yoon et al. [15]. C_g includes the upper electrode and the generated plasma over the dielectric surface, while C_d is the embedded electrode and the dielectric barrier. These capacitances are estimated as,

$$C_g \propto f(t_e, t_d, \epsilon_0, l_p) = 2\pi\epsilon_0 \frac{l_p}{\ln\left(\frac{0.5t_e + \lambda_d}{0.5t_e}\right)}; \quad (1)$$

$$C_d \propto f(t_e, t_d, \epsilon_d, l_e) = 2\pi\epsilon_d \frac{l_e}{\ln\left(\frac{0.5t_e + 2t_d}{0.5t_e}\right)} \quad (2)$$

The difference in the definition of the capacitance with that of [15] is the inclusion of the length of the embedded electrode length l_e , which is known, and the plasma region length l_p , which is unknown. Here, for simplicity the span wise length of the electrodes is assumed to be finite and equal to unity. And the considered cylindrical capacitors for each electrode are aligned in the stream wise direction. The schematic of the typical DBD actuator and the corresponding AC circuit is presented in Fig. 1, where the various lengths appearing in Eqs (1) and (2) are depicted. C_g and C_d capacitors are connected in a serial way to each other. Thus, the equivalent capacitance of the DBD actuator can be readily calculated as,

$$C_{eq} = \frac{C_g C_d}{C_g + C_d} \quad (3)$$

The Debye length (λ_D (m)) is estimated through the relation presented by Bouchmal [33] as,

$$\lambda_D = 0.2 \left(0.3 \times 10^{-3} V_{\text{app}} (\text{kV}) - 7.42 \times 10^{-4} \right) \quad (4)$$

in which V_{app} is the applied voltage in kilo Volts.

The property that governs if ionization occurs is the electric field (threshold value of at which the ionization occurs). To define this threshold value, the critical voltage at which the air is observed to first ionize (the critical voltage) is considered to be equal to the break down voltage V_{bd} , of the DBD. Yoon et al. [15] correlated the

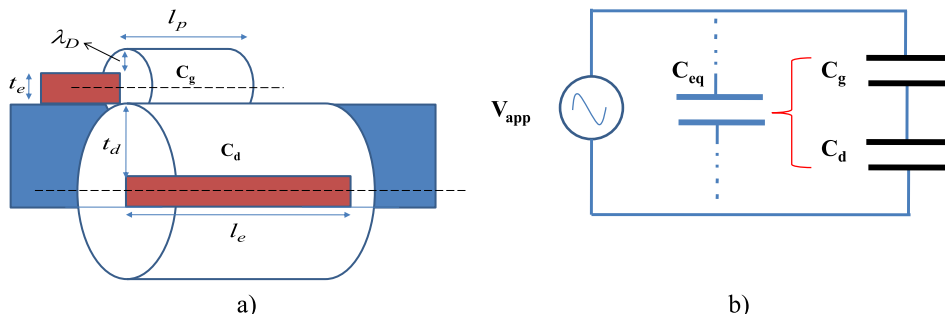


Fig. 1. a) Schematic of the considered DBD capacitor system. b) Equivalent circuit for the DBD plasma actuator system.

break down voltage taken as the initial operation voltage in the work of Thomas et al. [34] as,

$$V_{bd}(kV) = 4.8289 + (8.063145 \times 10^2 t_d). \quad (5)$$

where t_d (m) is the thickness of the dielectric. However it is well known that the break down voltage is dependent on the operating pressure p , the secondary emission coefficient γ and the dielectric thickness. an alternative relation, for calculating the break down voltage is adopted from the work of Ref. [35] as,

$$V_{bd}(V) = \pi B \sqrt{\frac{p(\text{Torr}) t_d(\text{cm}) \ln(1 + \gamma^{-1})}{2A}}. \quad (6)$$

where $A = 15 \text{ cm}^{-1} \text{ Torr}^{-1}$, $B = 365 \text{ V cm}^{-1} \text{ Torr}$ for air as working fluid. The effect of the plasma actuator arises through the electrostatic pressure which can be interpreted as the total energy consumption of the plasma actuator. The DBD plasma actuator was considered as a circuit with equivalent capacitance C_{eq} , thus the energy consumption of the plasma actuator over the period τ is related to the energy consumption (W) of the equivalent capacitance, calculated as,

$$l_p = \max \left[\left\{ \frac{2^{2/3} 40^{4/5} \left(2^{2/3} \rho f C_{d0}^2 C_{g0}^2 l_e^{10} (V_{app} - V_{bd})^2 (C_{g0} + C_{d0})^8 \right)^{1/5}}{40^2 (C_{g0} + C_{d0})^2} \right. \right. \\ \left. \left. \frac{0.0025}{l_g} \right] \quad (14)$$

$$W = \int_0^\tau VI \, dt = C_{eq} \int_0^\tau V \frac{dV}{dt} dt. \quad (7)$$

Plasma only discharges when the electric field strength (applied voltage (V_{app})) is larger than the critical value of electric field for the ionization to occur E_{cr} (the break down voltage (V_{bd})), and therefore, the consumed power (P) of the capacitance is estimated by taking the integration only in the effective plasma period (Δt) as,

$$W = \frac{1}{2} C_{eq} (V_{app} - V_{bd})^2; \quad (8)$$

$$\Delta t = \left(\frac{1}{2\pi f} \left[\frac{\pi}{2} - \sin^{-1} \left(\frac{V_{bd}}{V_{app}} \right) \right] \right) \approx \frac{1}{4f}; \quad (9)$$

$$P = \frac{W}{\Delta t} = 2f C_{eq} (V_{app} - V_{bd})^2. \quad (10)$$

where f is the frequency of the applied voltage. In the above equations, it was assumed that C_{eq} is the average equivalent capacitance over the effective plasma period. Moreover, In Eq. (9), the effect of voltage shape was ignored for the approximation of Δt . In fact, Eq. (10) provides an estimation of the area of the characteristic Lissajous figure of the DBD actuator. As we have already mentioned, the thrust generated by the DBD actuator is proportional to its power consumption, and thus,

$$T \cong 2\alpha f C_{eq} (V_{app} - V_{bd})^2. \quad (11)$$

where α is a fitting coefficient which is considered to be unity. Moreover the dimension of the region in which this thrust is effective is obtained from an experimental correlation presented by Ref. [15], as,

$$l_p = 0.005 \left(\frac{T}{0.04} \right)^{0.5}, \quad h_p = 0.0018 \left(\frac{T}{0.04} \right)^{0.5} \quad (12)$$

where l_p, h_p are respectively the length and the height of the plasma region in (m), and thrust T , is in (N/m).

However the dependency of thrust on the extension of the plasma region were observed in the experimental work of Durscher and Roy [36] to have to have a linear relation, with a minimum length for the plasma region of 2.5 mm. Thus, If we consider,

$$C_{g0} = \frac{C_g}{l_p}, \quad C_{d0} = \frac{C_d}{l_e}, \quad (13)$$

and replace the thrust in Eq. (12) from Eq. (17), the length of the plasma region is calculated directly as,

where l_p, l_g, l_e are in [m]; C_{g0}, C_{d0} [F/m] and V_{app}, V_{bd} in [V]. l_g is the asymmetric gap length between the trailing edge of the exposed electrode and the leading edge of the grounded electrode. Optimum gas spacing could higher thrust for the plasma actuator. Here, we have assumed that the minim length of the plasma region is equivalent to the gap spacing (if exists).

To approximate this dependency of the thrust on the power consumption, we assume a situation of uniform flow ($m' = \frac{dm}{dt} \approx cte$), this results in,

$$T = \frac{dm}{dt} v, \quad P = \frac{1}{2} \frac{dm}{dt} v^2, \quad \frac{dm}{dt} = \rho A v, \quad (15)$$

$$T = [4\rho A P^2]^{1/3}. \quad (16)$$

where A is the area of the actuator.

Substituting Eqs. (11) and (10) inside Eq. (16), we have an estimation of the thrust generated by plasma actuator,

$$T = \alpha \left[4\rho l_p \left(2f \frac{C_{g0} C_{d0} l_e l_p}{C_{g0} l_p + C_{d0} l_e} (V_{app} - V_{bd})^2 \right)^2 \right]^{1/3}. \quad (17)$$

The air density ρ in the above equation is calculated from the ideal gas law.

2.2. Numerical modeling of plasma generated body force

Since Eq. (17) already provides us with a correct scale for the thrust generated by the plasma, we only need the correct

distribution and direction of the body force generated by the plasma actuator to close the formulation of the model. The body force generated by the plasma actuator depends on the charge density (ρ_c) and the electric field (E) as expressed by,

$$\vec{F}_0 = \rho_c \vec{E} \quad (18)$$

With this and the Eq. (17), we define the scales for the charge density and the electric field as,

$$\rho_{c,\max} = 2fC_{eq} \frac{(V_{app} - V_{bd})}{f_{corr}\lambda_D}, \quad (19)$$

$$f_{corr} = \frac{1}{2} \sqrt{2\pi} \frac{\sigma}{l_p} \left[\operatorname{erf}\left(\frac{1}{2} \frac{\mu\sqrt{2}}{\sigma}\right) + \operatorname{erf}\left(\frac{1}{2} \frac{\sqrt{2}(l_p - \mu)}{\sigma}\right) \right]$$

$$\vec{E} = E_0 \vec{E}^* \quad E_0 = \frac{(V_{app} - V_{bd})}{l_p}, \quad (20)$$

where \vec{E} is the electrostatic field vector $\vec{E} = -\nabla\phi$, and the star indicates normalized fields. To arrive at Eq. (19), we have assumed that plasma is distributed uniformly in the span wise direction and the effective height of the equivalent capacitor that is storing the same charges is equal to the Debye length, and the accumulation of the charge occurs during the time interval Δt . Moreover, this effective height is corrected (with an error function) in a way to compensate for the charge density drop over the dielectric surface (Eq. (27)). Solution of the charge density field and the electric potential was based on the model developed in Ref. [29], with a modified boundary condition for the electric field on the surface of the dielectric layer. We should mention that a key advantage of the parameter scaling in Eqs. (19) and (20) is that the voltage dependency of power and body force can be predicted more accurately, and also that the model thus needs less unknown fitting parameters.

By considering Gauss law, we need to solve the following Poisson equation for the electric field,

$$\nabla \cdot (\epsilon \vec{E}) = \rho_c. \quad (21)$$

According to the split-potential field model, the electric potential is separated in two parts, one being a potential due to the external electric field, and the other being a potential due to the net charge density in the plasma,

$$\Phi = \phi + \varphi. \quad (22)$$

Assuming that the Debye length is small, as well as the charge on the wall above the encapsulated electrode, then the distribution of charged particles in the domain is governed by the potential due to the electric charge on the wall, being unaffected by the external electric field. The smaller the Debye length, the narrower the plasma region located near the electrode and dielectric surface becomes. Therefore, the governing equations for the potentials due to the external electric field and for the net charge density are,

$$\nabla \cdot (\epsilon \nabla \phi) = 0, \quad (23)$$

$$\nabla \cdot (\epsilon \nabla \varphi) = -\rho_c. \quad (24)$$

The charge density and Debye length are related by,

$$\frac{\rho_c}{\epsilon_0} \approx -\frac{\phi}{\lambda_D^2}. \quad (25)$$

and after replacing the above equation into Eq. (24), we obtain the governing equation for the net charge density is obtained,

$$\nabla \cdot (\epsilon_r \nabla \rho_c) = \frac{\rho_c}{\lambda_D^2}, \quad \epsilon = \epsilon_0 \epsilon_r \quad (26)$$

Eq. (23) is solved for the electric potential, using the applied voltage on the electrodes as boundary conditions. Applied AC voltage is imposed at the exposed electrode while the embedded electrode is prescribed as ground by setting the electric potential to zero. At the outer boundaries, $\partial\phi/\partial n = 0$ is assumed. Eq. (26) is solved for the net charge density on the air side of the domain. A zero normal gradient for the net charge density is imposed on the solid walls except in the region covering the lower electrode. The charge density is set to zero on the outer boundaries. To close the formulation of the model, the distribution of charge density on the surface of the dielectric, over the embedded electrode, is prescribed in the stream wise direction by a half Gaussian distribution function $G(x)$, which follows closely the experimental plasma distribution over the embedded electrode, that is,

$$G(x) = \exp\left(-\frac{(x - \mu)^2}{2\sigma^2}\right), \quad (27)$$

In Eq. (27), μ is the location parameter indicating the position of the maximum, and σ is a scale parameter determining the rate of decay. The location and scaling parameters depend on the voltage and operating characteristics of the DBD. We should mention that the correct distribution of the charge density on the dielectric surface ($\rho_{c,w} = \rho_{c,\max} G(x) f(t)$) can have a great influence on the accuracy of the simulation results. However, for the purpose of simplification of the computations, the assumption of a simple Gaussian distribution is viable. The location parameter is chosen such that the peak of charge density corresponds to the middle of the plasma region extension over the embedded electrode. In addition, the value of scaling parameter is selected in a way to allow a gradual decay of the charge density distribution to the end of the plasma region length. Moreover the dielectric shielding boundary condition introduced by Ibrahim and Skote [37] for the electric potential is also adopted which reads as,

$$\nabla_n \phi = \nabla_t \cdot (\lambda_D \epsilon_r \nabla_t \phi) \quad (28)$$

The condition produces a thin layer across the boundary that shields the electric field formed by the two electrodes, thus giving rise to the formation of the so called memory voltage on the dielectric surface.

3. Numerical procedure and flow solver

We note that Eqs. (23) and (26) do not contain a time derivative term. Only the boundary condition for the applied voltage at the exposed electrode and the boundary condition for the charge density at the dielectric surface are time dependent. Therefore, Eq. (23) can be normalized and be solved by imposing a constant boundary condition equal to unity at the upper electrode and similarly Eq. (26) can be normalized for charge density. The normalized parameters for two dimensional coordinates are as follows,

$$\rho_c^* = \frac{\rho_c}{\rho_{c,\max} f(t)}, \quad \phi^* = \frac{\phi}{\phi_{\max} f(t)}, \quad \vec{E}^* = \nabla \phi^* = l_p \left(\frac{\partial \phi^*}{\partial x} \vec{i} + \frac{\partial \phi^*}{\partial y} \vec{j} \right), \quad (29)$$

where $f(t)$ is a function representing the shape of the applied voltage.

Once the dimensionless distribution is determined, the dimensional values at any given time can be obtained by multiplying this

distribution with the corresponding normalization factor. In this manner, there is no need to solve the plasma model in an unsteady manner. The methodology is explained in detail in Ref. [23].

The interaction of the plasma actuator is implemented as an explicit source term inside the momentum equation. The flow governing equations were solved by finite volume method using the Commercial CFD solver FLUENT. The plasma model was then coded as an UDF (User Defined Function) and was used alongside for the simulation purpose. Two dimensional Cartesian orthogonal grid were used for the numerical simulation. Note that the grid spacing should not be larger than the Debye length. For enforcing this and reaching grid independency of the obtained results, and also reducing the numerical cost, the numerical grid was refined toward the electrodes and surface of dielectric layer. Moreover, the grid was refined in the regions where higher values of electric field and charge density exist. Thus, the grid spacing was stretched toward the electrode both in the normal direction and in the stream wise direction leading to the minimum cell size of about 2 μm . The total number of the cells varies for the different test cases as the size of the computational domain varies.

4. Results and discussion

For the purpose of validation and to ascertain the improvement due to this new modeling approach, three different test cases have been selected. The first validation test case is the experimental work of Thomas et al. [34], upon which the experimental correlation of the plasma extension is based. Table 1, presents the details of the DBD plasma actuator used in that work of Thomas et al. [34]. The computational grid of this case (Mesh A) consists of around 47×10^4 cells for a rectangular domain of $1.1 \text{ m} \times 0.5 \text{ m}$.

Fig. 2a) shows the comparison of the scaled calculated thrust and experimental results of Thomas. It is clear that model provides the correct trends regarding the influence of the different effective components of DBD actuator. Also, the model reasonably predicts the nonlinear dependency of the thrust and applied voltage although the rate of increase of the data is somewhat lower than the predictions. It should be mentioned that, considering the simplicity of the model, the difference between the calculated and experimental results is reasonable and in line with experimental results. In Fig. 2b), the correlation between the applied voltage and thrust dependency is depicted. As shown in Ref. [30] the voltage and thrust are related through $T \propto V_{\text{app}}^{7/2}$, and here we have calculated this to be $T \propto V_{\text{app}}^{6.54/2}$. It is interesting to note that the thrust data of [34] in Fig. 2a) shows an even smaller rate of variation with voltage.

Moreover, a comparison between the unmodified split-potential model and the present modified model shown in Fig. 3, reveals that much improved level of agreement is achieved. The addition of the scaling to the model clearly modifies and improves the results. We should mention that for the unmodified model the values of the $\rho_{c,\text{max}}$ and λ_D were taken from the work of Suzen et al. [29] being 0.0008 C/m^3 and 0.001 m respectively.

Table 1
Details of the first validation test case (Thomas et al. [34]).

	Dielectric material	ϵ_{rd}	l_e (cm)	t_e (μm)	t_d (mm)	f (kHz)
A-	Teflon	2.0	5.08	40.0	3.18, 6.35	2.1
B-	Derlin	3.5	5.08	40.0	6.35	2.3
C-	Quartz	4.2	5.08	40.0	6.35	2.3
D-	Kapton	3.9	5.08	40.0	0.15	4.4
E-	Macor	6.0	5.08	40.0	3.18	2.3

For the second test case, we selected the experimental work of Durscher and Roy [36] in order to examine the predicting capability of the model in a range of the experimental data outside that used for the fitting of Eq. (12), which was, we recall, correlated from experimental results of Thomas et al. [34]. The DBD plasma actuator used in the experiments of [36] includes an exposed electrode with a length of 0.5 cm and an embedded electrode with length of 2 cm. Both electrodes were built from 70 μm thick copper strips. Also, the dielectric was 3 mm thick layer of acrylic with relative permittivity of 3.0. The computational domain for this case (Mesh B) was a rectangular with the dimension of $1.0 \text{ m} \times 0.5 \text{ m}$ with around 3.1×10^4 grid cells. Fig. 4 compares the thrust calculated by the present model and the experimental results of Durscher and Roy [36] for two frequencies over a range of applied voltage. The computed thrust is in reasonable agreement with the experimental results and thus confirming that the considered correlations been proposed are sufficiently general for thrust estimation outside of the range of parameters on which they were based.

Fig. 5 depicts the normalized electric potential distribution around the electrodes along with the normalized distribution of the charges over the surface of the dielectric material. It should be mentioned that the effect of finite electrode thickness is considered just for the scaling of the body force, as explained in the previous section, while the actual numerical domain for simulations assumes infinitely thin electrodes. In addition, In Fig. 5c), illustrates the induced ionic wind by means of the contour of velocity magnitude and velocity vectors are shown. The direction of most of the induced flow is in stream wise direction because the vertical component of the force generated by the plasma actuator is smaller than the horizontal component. Since the spatial distribution of the generated plasma body force and the ionic wind are obtained numerically, different actuators arrangement and electrode geometries could be modeled and analyzed easily.

In Fig. 6, calculated profiles of the steam wise velocity component are compared with the PIV data of Durscher and Roy [36] at two stations, $x = 25$ and 35 mm for $V_{\text{max}} = 10 \text{ kV}$, $f = 14 \text{ kHz}$. The trend is well captured but there is a difference between the maximum values of the velocities for both profiles. This is related to the under estimation of the thrust computed by the present model for the applied voltage (as can be seen in Fig. 4). However, for a simplified model the accuracy is acceptable and the predictions are in line with the experiments. Moreover, the figure shows that the position of the maximum velocity is predicted correctly by the present model.

One of the parameters that is known to affect the thrust is the length of the plasma region, which was estimated by Eq. (14). The obtained plasma region length from the present model was then compared with experimental results of Durscher and Roy [36], and the results are shown in Fig. 7. As can be seen the experimental results show approximately a linear relation between thrust and plasma region length while the numerical calculation is showing a quadratic tend. The deviation of the estimated scaled thrust (under estimation at low voltages, and over estimation at high voltages) is related to this point, i.e. the correct evaluation of the flow regime.

Finally, the experimental and numerical work of Palmeiro [32] is considered to compare the present model with other models and with experiment results. Three test cases are considered following [32], with different electrode geometry and applied voltage and some of their details are tabulated in Table 2. As shown in Ref. [32], the existing phenomenological models have diverse accuracy for different cases.

Table 3 compares the maximum velocity obtained from the present model with other phenomenological models and the experiments. It is obvious from this table that although our model is simple, it offers a more uniform predictive capability for the various

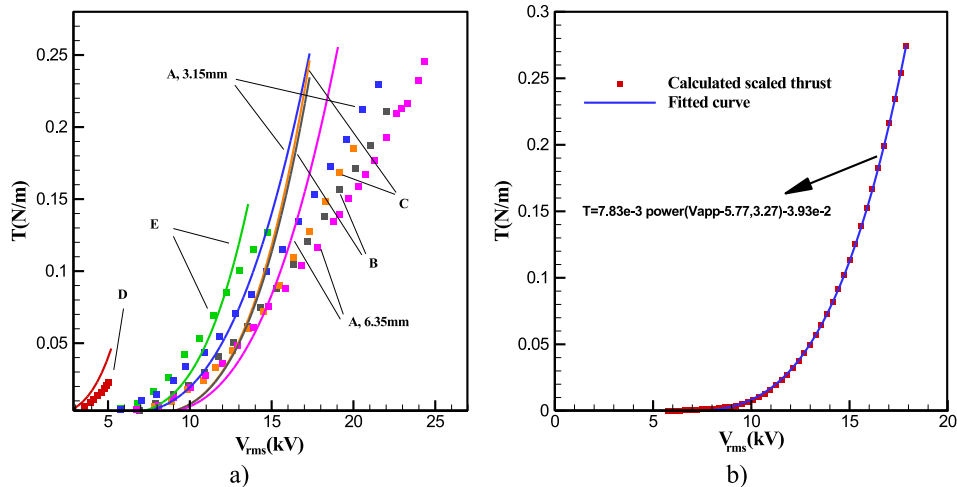


Fig. 2. a) Comparison of the computed scaled thrust (solid lines) with the experimental results of [34] (symbols). b) Correlation between the voltage and the calculated scaled thrust for the 6.35 mm thick Teflon material.

test cases compared with the other models. The maximum velocity shown in Table 3 is obtained at a specified stream wise measuring location which was equal to 10 mm, 10 mm, and 5 mm from the leading edge of the exposed electrode, respectively for cases (1), (2) and (3). The present model shows acceptable accuracy for all the three cases. Although the hybrid model of Lemire et al. [31] shows good accuracy for two of the cases, it is not capable of replicating the experimental results of the other case.

In Fig. 8 the obtained x -velocity profiles at the measuring locations mentioned above are compared with experimental and numerical results of Palmeiro [32]. The velocity profiles for each measuring station and modeling methods are normalized by the corresponding maximum velocity. For each case four sets of results are presented, namely A) the experimental results [32]; B) unmodified split-potential model; C) the model giving the closest behavior to the experiments; D) and the results obtained from the present model. After removing the discrepancies introduced by the correct prediction of the velocity peak, we see that our model is the

best to predict test cases (2) and (3), and none of the models is able to predict adequately the very narrow boundary-layer behavior of test case (1).

4.1. Effect of altitude on the thrust generation of plasma actuators

For a flow control system to be used in real applications, for which the altitude, for example, will vary significantly the characteristics of the thrust generated by the plasma actuators under various ambiental parameters need to be assessed to prove that they have adequate capability of usage. When the altitude of the aeronautical system is changed, several prosperities, including pressure, temperature and humidity, will change. These factors could alter various parameters of the plasma actuator system. As an example, the dielectric permittivity, secondary emission coefficient of the surface of the dielectric material, space ionization and attachment coefficient are dependent on local characteristics of the environment. The results of such assessment will serve to help the

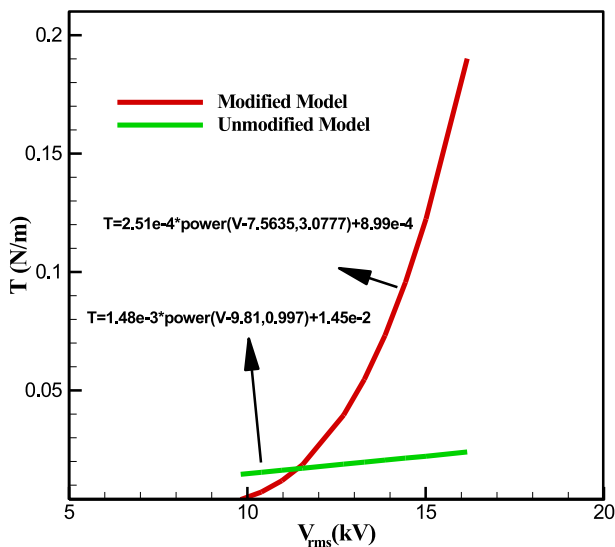


Fig. 3. Comparison between the numerically obtained thrust from the present modified model (which is more accurate) and the previous unmodified split-potential model.

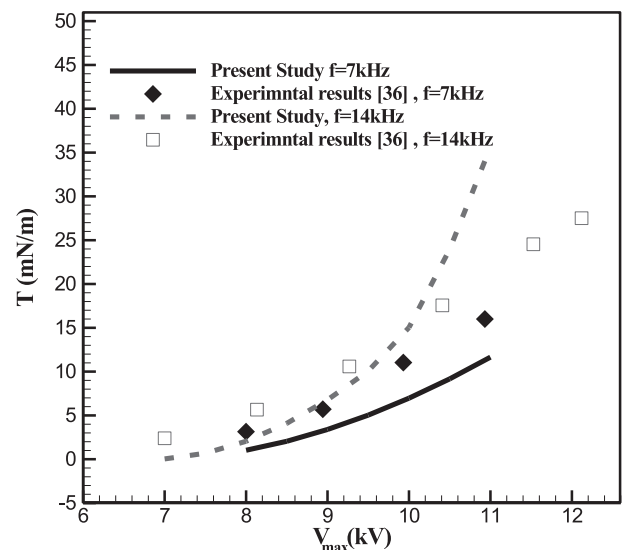


Fig. 4. Comparison between the calculated thrust from the present modified model and the experimental results of Durscher and Roy [36].

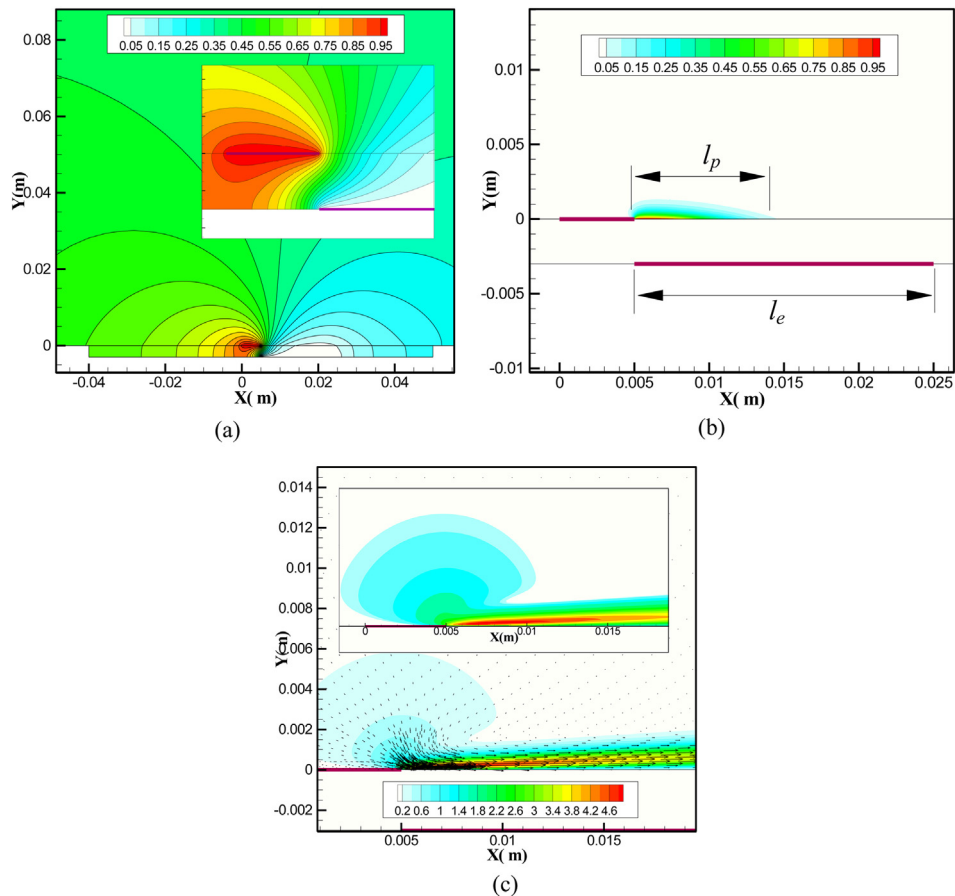


Fig. 5. a) Electric potential field around the DBD actuator for $V_{\max} = 10$ kV, $f = 14$ kHz. b) Charge density distribution over exposed electrode. c) Induced ionic wind velocity magnitude contour (m/s).

design of a novel flow control system using DBD plasma actuators, for high altitude airships which consists of both cruiser and feeder airship, with a wide range of change of altitude [38].

Several studies addressed the influence of the variation of altitude, temperature and relative humidity, such as [39] who concluded that the effectiveness of the actuator increases with

relative humidity also authors [27,40–44] studied the influence of the operating pressure on the performance of the plasma actuator. Wu et al. [40] considered the reduction of the operating pressure below atmospheric pressure level. They showed that the reduction of operating pressure causes a decrease of the rotational temperature of the electrons, and also an initial decrease in vibrational

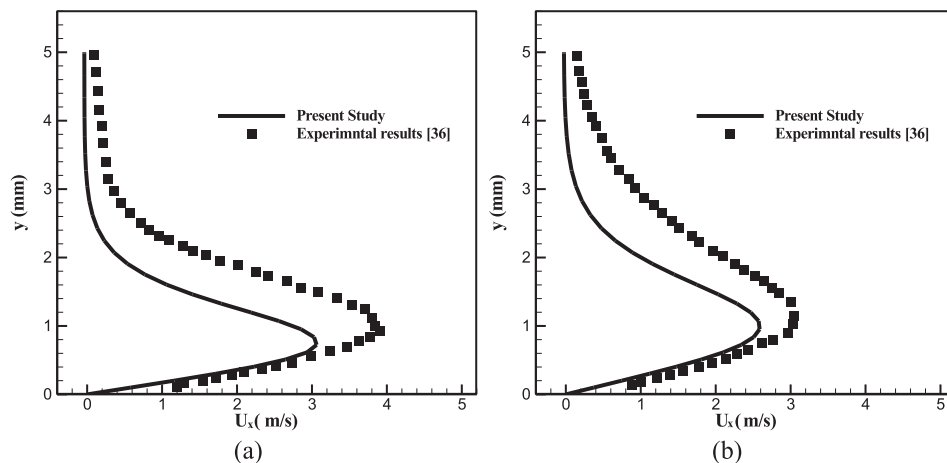


Fig. 6. Comparison between the calculated profile of the horizontal velocity and the experiments of Durscher and Roy [36]. At a) $x = 25$ mm. b) $x = 35$ mm, downstream of the exposed electrode.

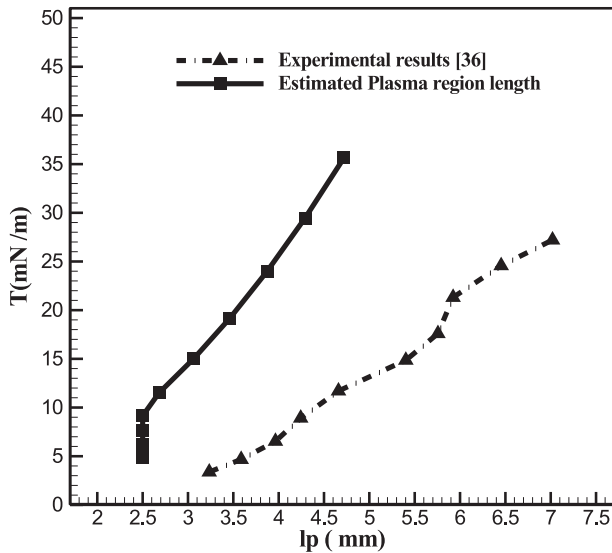


Fig. 7. Comparison of the estimated length of the plasma zone and the experimental results of Durscher and Roy [36].

temperature of the electrons followed by an increase. They also observed that the pressure reduction causes a change of the discharge mode at a transition pressure of 45 torr. Litvinov et al. [41] mentioned that the larger thrust resulting from a decrease in pressure could be associated with an increase in the plasma volume, ahead of the electrodes, allowing for a larger total number of ions, moreover, it was shown that the relative area occupied by the plasma on the dielectric surface varies with pressure as $(p_0(200 \text{ torr})/p)^{7/5}$. Benard et al. [42] also showed that the plasma extension increases when reducing the operating pressure. Their results revealed that the extension of the plasma region was smaller than the length of the embedded electrode, when the pressure is equal to 1 atm (in accordance to the assumption we made in previous Section 2), however, when the operating pressure is reduced the plasma tended to extend more.

Abe et al. [44] investigated the effect of operating pressure on the plasma actuators performance and reported the same result, the power consumption of the DBD increases with a decrease of pressure. In essence, pressure influences the thrust generating capability of the plasma actuator by decreasing the voltage required to create a discharge (Eq. (6)). In other words, when the gas density is reduced, current pulses become more intense as the electric field is kept constant and fewer collisions between charged particles and surrounding neutrals occur. Versailles et al. [45] looked to the effect of pressure in a range above atmospheric pressure. They concluded that, for a given actuator input, the plasma density and extent tends to decrease with increasing pressure.

For the purpose of examining the ability of the proposed model to capture the effect of altitude on the thrust produced by the plasma actuator, several test cases were considered. Table 4 shows

Table 2
Details of the test cases of Palmeiro [32].

Test case	ϵ_{rd}	l_e (mm)	l_g (mm)	t_d (mm)	f (kHz)	V_{max} (kV)
(1)	2.9	6.35	1.0	0.19	3.0	6.0
(2)	2.9	12.7	1.0	0.57	3.0	7.5
(3)	2.9	5.0	0	0.18	2.75	5.0

Table 3
Maximum induced velocity U_{max} (m/s).

Test case	Experiments [32]	Simple body force model [28]	Split-potential model [29]	Lumped-circuit model [21]	Hybrid model [31]	Present model
(1)	1.9458	0.7266	0.2110	8.9311	1.5339	1.05642
(2)	1.2772	0.8383	0.2495	7.3674	0.2927	1.10435
(3)	1.5181	0.3042	0.2124	3.9770	1.2382	0.959561

the geometrical details of the actuators employed for testing the effect of operating pressure. The first test case is related to pressures below the atmospheric pressure level, and the second is related to pressures above the atmospheric level.

Eq. (17) provides us with the thrust exerted by a unit mass of working fluid, per unit length of plasma region. Moreover, using Eq. (18), source term for the momentum equations of air with density of ρ , the thrust which is generated by the force induced by the plasma actuator on the surface can be numerically calculated.

An extra correction needs to be done for the Debye length. Valerioti et al. [7], considered a pressure dependency of the Debye length as $\lambda_D \propto p^{(-4/3)}$. Debye Length is related to the electron charge density and electron temperature as $\frac{1}{\lambda_D} \cong \left[\frac{e^2 n_e}{\epsilon_0} \left(\frac{1}{k_B T_i} + \frac{1}{k_B T_e} \right) \right]^{1/2}$. We have fitted the variation of the electron density and electron temperature with operating pressure from the work of Wu et al. [40]. We have obtained the Debye length dependency to operating pressure as $\lambda_D \propto p^{(-3/5)}$ by replacing the fitting of the electron density and electron temperature in the formula of the Debye length and then replaced in the mentioned equation, resulting in the dependency of the Debye length on operating pressure.

In Fig. 9 the variation of the normalized thrust obtained from (Eq. (17)) and normalized body force (from Eq. (18)), with decreasing pressure is presented for this case. As indicated in this figure both parameters possess a maximum point, whose value is in accordance with the results presented by Refs. [40,42,44]. The peaks of the scaled thrust and body force, estimated by Eqs. (17) and (18) are occurring respectively at 0.59 atm and 0.71 atm, while the experimental results suggest a peak at 0.6 atm. However, the main point is that the simple model presented here could capture the behavior of thrust correctly.

For test case P1, the velocity profiles obtained at different stream wise sections over the plasma actuator, are presented in Fig. 10. The maximum value of the induced velocity is in accordance with the experimental results for this case at atmospheric pressure.

For the case in which operating pressure is higher than the atmospheric pressure, the thrust obtained from the present study is compared with the experimental results of [45]. For pressures higher than atmospheric pressure, no pressure correction for the Debye length is considered. The results are plotted in Fig. 11 and show the correct trend: reduction of the thrust by increasing the pressure. As was explained at Ref. [45], increase in operating pressure in constant temperature causes an increase in air density. Therefore the mean free path between the particles and the kinetic energy of them when they collide reduces. Thus the rate of the momentum transfer decreases. Secondly the ignition voltage (break down voltage) is increasing with increase in operating pressure. Thus at higher operating pressure, the voltage needed for the plasma region to form is larger. In this study, the secondary electron emission (γ), was considered constant and equal to 0.01. In fact, γ depends on surface characteristics, ionization energy, and primary electron energy. As shown by Wu et al. [40], when the operating pressure is changed the electron energy and temperature

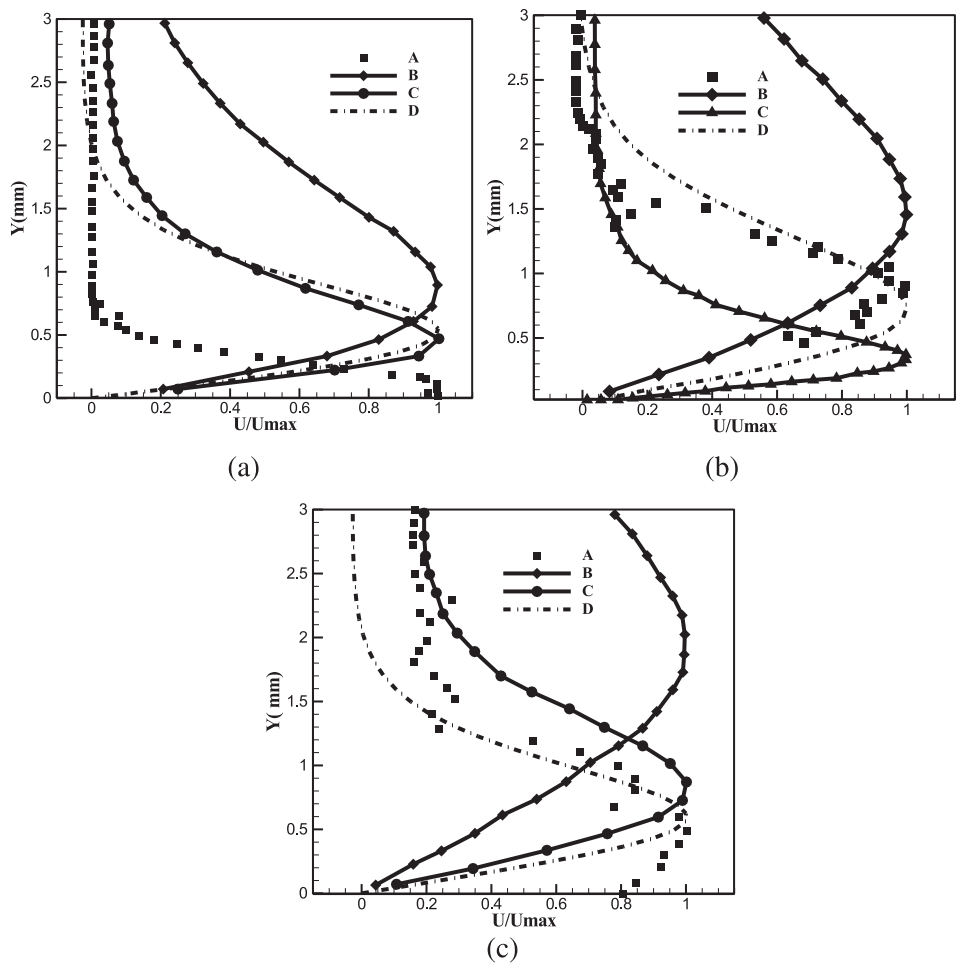


Fig. 8. Comparison of the x-velocity profile at the specified measuring location a) Case (1) b) Case (2) c) Case (3).

will change. Thus, it may be expected that the secondary electron emission γ would also be depend on pressure. To approximate the sensitivity of the results to the level of γ , in Fig. 11 the estimated thrust is shown for two values of γ and the lower $\gamma = 0.001$ seems to offer results closer to the experiments in which pressure varies in a range $p = 150\text{--}250\text{ kPa}$.

5. Conclusions

A simple model for plasma discharge and its effect on the flow was developed based on scaling the thrust generated by DBD plasma actuators. The scaled thrust model correctly predicts the nonlinear dependency of the thrust produced and the applied voltage. These scales were then introduced into a simple phenomenological model to estimate and simulate the body force distribution generated by the plasma actuator. Although the model includes some experimental correlations, it does not need any fitting parameter. The model was validated with experimental

results and showed better accuracy compared to previous plasma models. Moreover, the generality of the model was confirmed through validation with three different experiments. Finally, the model was tested for predicting the thrust for cases in which the altitude (pressure) is changing.

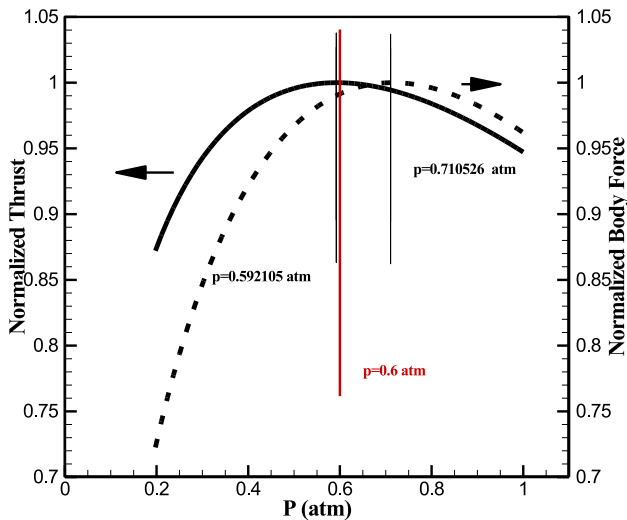


Fig. 9. Variation of normalized thrust and force with decreasing pressure (below atmospheric).

Table 4
Case details – effect of operating pressure.

Test case	t_e (mm)	l_e (mm)	l_g (mm)	t_d (mm)	ϵ_d	Dielectric material
P1 [42]	0.1	10	5	4	3	PMMA
P2 [45]	0.076	12.7	2	1.6	2	Teflon

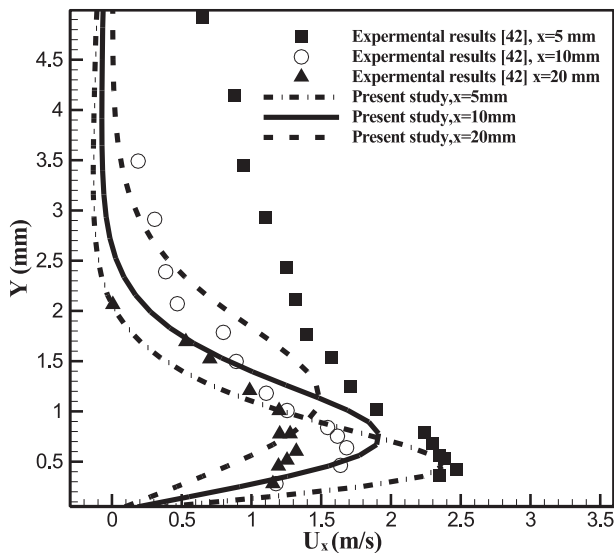


Fig. 10. Velocity profile at different stream wise sections for atmospheric pressure, $p = 1$ atm.

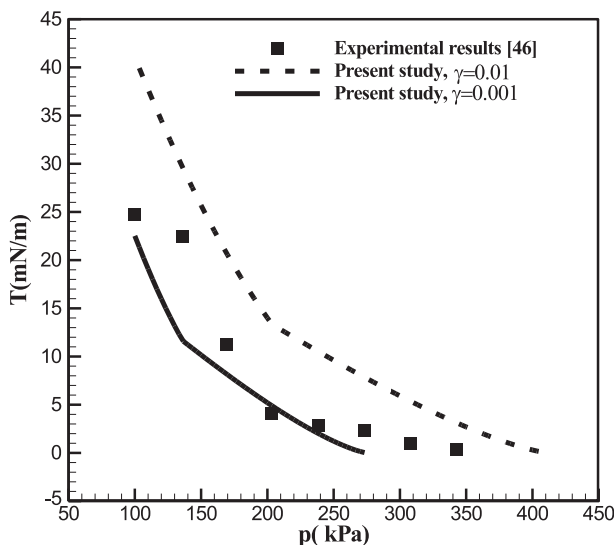


Fig. 11. Comparison of the effect of higher atmospheric pressure on thrust estimated by the present study with the results obtained in Ref. [45].

Acknowledgments

The present work was performed as part of Project MAAT, supported by European Union on course of the 7th Framework Programme under the grant number 285602. Part of the work was also supported by C-MAST – Center for Mechanical and Aerospace Sciences and Technologies, Fundação para a Ciência e a Tecnologia (Portuguese Foundation for Science and Technology) Research Unit No. 151.

References

- [1] M. Abdollahzadeh, J.C. Páscoa, P.J. Oliveira, Numerical investigation on efficiency increase in high altitude propulsion systems using plasma actuators, in: ECCOMAS 2012-Eur. Congr. Comput. Methods Appl. Sci. Eng., 2012, pp. 6563–6581.
- [2] W. Liu, L. Jia, W. Yan, F. Kong, Y. Hao, Study on the glow discharge in the atmospheric pressure, *Curr. Appl. Phys.* 11 (2011) S117–S120.

- [3] T. Matsunuma, T. Segawa, Effects of input voltage on flow separation control for low-pressure turbine at low Reynolds number by plasma actuators, *Int. J. Rotating Mach.* 2012 (2012) 1–10.
- [4] M.M. Hollick, M. Arjomandi, B.S. Cazzolato, An investigation into the sensory application of DBD plasma actuators for pressure measurement, *Sensors Actuat. A Phys.* 171 (2011) 102–108.
- [5] H. Nishida, T. Abe, Numerical analysis of plasma evolution on dielectric barrier discharge plasma actuator, *J. Appl. Phys.* 110 (2011) 013302.
- [6] T. Shao, H. Jiang, C. Zhang, P. Yan, M.I. Lomaev, V.F. Tarasenko, Time behaviour of discharge current in case of nanosecond-pulse surface dielectric barrier discharge, *EPL Europhys. Lett.* 101 (2013) 45002.
- [7] J.A. Valerioti, T.C. Corke, Pressure dependence of dielectric barrier discharge plasma flow actuators, *AIAA J.* 50 (2012) 1490–1502.
- [8] M. Abdollahzadeh, J.C. Páscoa, P.J. Oliveira, Two-dimensional numerical modeling of interaction of micro-shock wave generated by nanosecond plasma actuators and transonic flow, *J. Comput. Appl. Math.* 270 (2013) 401–416.
- [9] J.P. Boeuf, Y. Lagmich, T. Unfer, T. Callegari, L.C. Pitchford, Electrohydrodynamic force in dielectric barrier discharge plasma actuators, *J. Phys. D: Appl. Phys.* 40 (2007) 652–662.
- [10] M.J. Pinheiro, A.A. Martins, Electrical and kinetic model of an atmospheric rf device for plasma aerodynamics applications, *J. Appl. Phys.* 108 (2010) 033301.
- [11] A.V. Likhanskii, M.N. Shneider, S.O. Macheret, R.B. Miles, Modeling of dielectric barrier discharge plasma actuator in air, *J. Appl. Phys.* 103 (2008) 053305.
- [12] J. Bai, J. Sun, Q. Zhang, D. Wang, PIC simulation of RF hydrogen discharges in a transverse magnetic field, *Curr. Appl. Phys.* 11 (2011) S140–S144.
- [13] T. Unfer, J.-P. Boeuf, F. Rogier, F. Thivet, Multi-scale gas discharge simulations using asynchronous adaptive mesh refinement, *Comput. Phys. Commun.* 181 (2010) 247–258.
- [14] M.M. Bermudez, R. Sosa, D. Grondona, A. Márquez, H. Kelly, G. Artana, Study of a pseudo-empirical model approach to characterize plasma actuators, *J. Phys. Conf. Ser.* 296 (2011) 012023.
- [15] J.-S. Yoon, J.-H. Han, Semi-empirical thrust model of dielectric barrier plasma actuator for flow control, *J. Aerosp. Eng.* (2013) 1934–5525.
- [16] A. Abdoli, I. Mirzaee, A. Anvari, N. Purnahmod, Simulation of body force field effects on airfoil separation control and optimization of plasma actuator, *J. Phys. D: Appl. Phys.* 41 (2008) 175204.
- [17] D.M. Orlov, T.C. Corke, Numerical simulation of aerodynamic plasma actuator effects, in: 43rd AIAA Aerosp. Sci. Meet. Exhib. 10, AIAA 2005-1083, 2005, pp. 1–12.
- [18] D.V. Gaitonde, M.R. Visbal, S. Roy, Control of flow past a wing section with plasma-based body forces, in: 36th AIAA Plasmadynamics Lasers Conf., AIAA 2005-5302, 2005, pp. 1–14.
- [19] S. Lemire, H.D. Vo, Reduction of fan and compressor wake defect using plasma actuation for tonal noise reduction, *J. Turbomach.* 133 (2011) 011017.
- [20] D.M. Orlov, T.C. Corke, Electric circuit model for aerodynamic plasma actuator, in: 44th AIAA Aerosp. Sci. Meet. Exhib. 9–12 January 2006 Reno Nevada, 2006, pp. 9–12.
- [21] B.E. Mertz, Refinement, Validation, and Implementation of Lumped Circuit Element Model for Single Dielectric Barrier Discharge Plasma Actuators (Ph.D. thesis), University of Notre Dame, 2010.
- [22] V.R. Soloviev, Analytical estimation of the thrust generated by a surface dielectric barrier discharge, *J. Phys. D: Appl. Phys.* 45 (2012) 025205.
- [23] M. Abdollahzadeh, J.C. Páscoa, P.J. Oliveira, Numerical modeling of boundary layer control using dielectric barrier discharge, in: Conferência Nac. Em Mecânica Dos Fluidos, Termodinâmica e Energ. MEFE, 2012, pp. 1–10. Paper No 61.
- [24] I. Maden, R. Maduta, J. Kriegseis, S. Jakirlić, C. Schwarz, S. Grundmann, et al., Experimental and computational study of the flow induced by a plasma actuator, *Int. J. Heat Fluid Flow* 41 (2013) 80–89.
- [25] I. Maden, J. Kriegseis, R. Maduta, S. Jakirli, C. Schwarz, S. Grundmann, et al., Derivation of a plasma-actuator model utilizing quiescent-air PIV data, in: Proceeding 20th Annu. Conf. CFD Soc. Canada, Alberta, Canada, 2012.
- [26] J. Kriegseis, C. Schwarz, C. Tropea, S. Grundmann, Velocity-information-based force-term estimation of dielectric-barrier discharge plasma actuators, *J. Phys. D: Appl. Phys.* 46 (2013) 055202.
- [27] N. Benard, A. Debien, E. Moreau, Time-dependent volume force produced by a non-thermal plasma actuator from experimental velocity field, *J. Phys. D: Appl. Phys.* 46 (2013) 245201.
- [28] W. Shyy, B. Jayaraman, A. Andersson, Modeling of glow discharge-induced fluid dynamics, *J. Appl. Phys.* 92 (2002) 6434.
- [29] Y. Suzen, G. Huang, J. Jacob, D. Ashpis, Numerical simulations of plasma based flow control applications, in: 35th AIAA Fluid Dyn. Conf. Exhib., 2005, pp. 1–11.
- [30] M.L. Post, Plasma Actuators for Separation Control on Stationary and Oscillatory Airfoils (Ph.D. thesis), University of Notre Dame, 2004.
- [31] S. Lemire, H.D. Vo, M.W. Benner, Performance improvement of axial compressors and fans with plasma actuation, *Int. J. Rotating Mach.* 2009 (2009) 1–13.
- [32] D. Palmeiro, Modeling of Dielectric Barrier Discharge Plasma Actuators (Master thesis), University of Toronto, 2011.
- [33] A. Bouchmal, Modeling of Dielectric-Barrier Discharge Actuator (Master of Science thesis), Delft University of Technology, 2011.
- [34] F.O. Thomas, T.C. Corke, M. Iqbal, A. Kozlov, D. Schatzman, Optimization of dielectric barrier discharge plasma actuators for active aerodynamic flow control, *AIAA J.* 47 (2009) 2169–2178.

- [35] V.R. Soloviev, V.M. Krivtsov, Phenomenological model of the body force induced by surface dielectric barrier discharge, in: 49th AIAA Aerosp. Sci. Meet. Incl. New Horizons Forum Aerosp. Expo., Orlando, Florida, 2011, pp. 1–14.
- [36] R. Durscher, S. Roy, Evaluation of thrust measurement techniques for dielectric barrier discharge actuators, *Exp. Fluids* 53 (2012) 1165–1176.
- [37] I.H. Ibrahim, M. Skote, Simulations of the linear plasma synthetic jet actuator utilizing a modified Suzen-Huang model, *Phys. Fluids* 24 (2012) 113602.
- [38] A. Dumas, M. Madonia, I. Giuliani, M. Trancossi, MAAT Cruiser/Feeder Project: Criticalities and Solution Guidelines, SAE Tech. Pap. 01, 2011, p. 2784.
- [39] R. Anderson, S. Roy, Actuators using dry and humid air, in: 44th AIAA Aerospace Sciences Meeting and Exhibit, AIAA R. Anderson, S. Roy, Actuators using dry and humid air (pp. 1–9, in:). 44th AIAA Aerospace Sciences Meeting and Exhibit, AIAA 2006-0369, 2006, pp. 1–9.
- [40] Y. Wu, Y. Li, M. Jia, H. Song, Z. Guo, X. Zhu, et al., Influence of operating pressure on surface dielectric barrier discharge plasma aerodynamic actuation characteristics, *Appl. Phys. Lett.* 93 (2008) 031503.
- [41] V.M. Litvinov, V.V. Skvortsov, A.A. Uspenskii, Role of the static pressure in experiments on flow control by means of surface capacitor discharges, *Fluid Dyn.* 41 (2006) 286–291.
- [42] N. Benard, N. Balcon, E. Moreau, Electric wind produced by a surface dielectric barrier discharge operating in air at different pressures: aeronautical control insights, *J. Phys. D: Appl. Phys.* 41 (2008) 042002.
- [43] J.W. Gregory, C.L. Enloe, G.I. Font, T.E. McLaughlin, S. Member, Force production mechanisms of a dielectric-barrier discharge plasma actuator, in: 45th AIAA Aerospace Sciences Meeting and Exhibit, AIAA 2007-185, 2007, pp. 1–13.
- [44] T. Abe, Y. Takizawa, S. Sato, A parametric experimental study for momentum transfer by plasma actuator, in: 45th AIAA Aerosp. Sci. Meet. Exhib., AIAA 2007-187, 2007, pp. 1–11.
- [45] P. Versailles, V. Gingras-Gosselin, H.D. Vo, Impact of pressure and temperature on the performance of plasma actuators, *AIAA J.* 48 (2010) 859–863.